IEEE Access
Multidisciplinary | Rapid Review | Open Access Journal

Received September 23, 2020, accepted October 4, 2020, date of publication October 8, 2020, date of current version October 21, 2020.

Digital Object Identifier 10.1109/ACCESS.2020.3029740

Traction Synchronous Homopolar Motor: Simplified Computation Technique and Experimental Validation

VLADIMIR DMITRIEVSKII[1], VLADIMIR PRAKHT[1], (Member, IEEE), ALECKSEY ANUCHIN[2], (Senior Member, IEEE), AND VADIM KAZAKBAEV[1]
[1]Department of Electrical Engineering and Electric Technology Systems, Ural Federal University, 620002 Yekaterinburg, Russia
[2]Department of Electric Drives, Moscow Power Engineering Institute, 111250 Moscow, Russia

Corresponding author: Alecksey Anuchin (anuchinas@mpei.ru)

This work was supported by the Russian Science Foundation under Grant 16-19-10618.

ABSTRACT Synchronous homopolar motors (SHMs) have been attracting the attention of researchers for many decades. Various mathematical models of SHM have been proposed to deal with its complicated magnetic circuit. Among them, there are time-consuming 3D finite element models (FEM), equivalent circuit models neglecting some significant features of the machine design, and 2D FEM models with virtual excitation winding distorting its magnetic field picture. This paper proposes a novel 2D FEM of SHM and shows that since there are no sources of excitation in the cross-sections of the rotor and stator stacks, no virtual elements are required. This model uses the general solution of the Gauss's law for magnetism containing excitation flux. The model is based on a set of magnetostatic boundary value problems for various rotor positions. The set of boundary problems is completed with the excitation equivalent circuit. The losses in the armature and field windings and the stator and rotor magnetic cores are computed in postprocessing. All these computations are carried out for a single combination of stator and rotor stack. A symmetrization algorithm is proposed to extend the obtained results to the whole SHM. A comparison of the theoretical and experimental data for a nine-phase three-section 320 kW SHM is carried out. These SHMs were used in a mining truck with a carrying capacity of 90 tons.

INDEX TERMS AC machines, automotive applications, brushless motors, electric vehicles, electromagnetic modeling, mining industry, traction motor.

I. INTRODUCTION

The synchronous homopolar motor (SHM) has been used in specific applications for over a century. The main advantage of the SHM is its simple and reliable construction with its brushless excitation located at the stator of the machine together with the armature winding. SHMs are utilized as generators in traction applications [1], aircrafts and trains [2], welding inverters [3], [4], etc. Their usage has been considered in kinetic energy storage systems [5] due to their ability to regulate flux. Moreover, in [6], [7] and [8], SHMs were used as traction motors. They can be utilized in high temperature and hazard environments as drives [9] and as high-power wind generators [10].

The associate editor coordinating the review of this manuscript and approving it for publication was Sanjeevikumar Padmanaban.

The SHM involves a complex configuration of the magnetic system, which is inconvenient for computation and optimization since magnetic flux changes its direction in three dimensions. In some parts of the motor, flux flows in the axial direction, while in other parts, it flows in the transverse plane and changes its direction to the axial one when coming from laminated parts to the stator back iron or the magnetic sleeve on the rotor shaft. Therefore, the finite element model (FEM) in 3D was used to compute the operation points of these motors [1], [11], [12].

The experimental verification of the 3D FEM computation was performed in [11] for the 0.75 kW, 3600 rpm SHM. However, only a limited analysis was performed due to the huge complexity of computations. Flux linkages were computed for two configurations of the motor. The performance characteristics were evaluated in [12] using 3D FEM for the

10 kW, 24 krpm SHM with an external rotor configuration. However, no verification of the model and no computation time estimation were introduced. The SHM and wound rotor synchronous machine were compared in a low power generation application in [1] using 3D FEM, and experimental validation was performed.

3D FEM ensures high accuracy but requires huge computation resources, which makes it nearly impossible to design and optimize the SHM using genetic algorithms or other optimization methods. Therefore, methods to simplify the computations using 2D models were introduced.

The virtual excitation coils were added to each rotor teeth in [1] and [13] to represent excitation flux in a 2D model. In the axial direction, the magnetic system was evaluated using analytical equations for the lumped parameters circuit. It was shown that the proposed approach can be used to estimate inductance and EMF in an idle mode of operation. Similar approaches and results were considered in [14].

The 2D FEM can be replaced with a detailed equivalent circuit. The equivalent magnetic circuit was developed for a low power synchronous homopolar generator in [5]. The advantage of this approach is the absence of the virtual excitation windings at the rotor teeth to simulate the field winding. Thus, a tolerable match of 3D FEM to the equivalent circuit method is shown. However, the noticeable mismatch between methods appears in some motor parameter configurations.

The comparison of the efforts of the computation under 3D FEM and equivalent circuit models is investigated in [15] for the SHM. It was shown that the 3D FEM requires 10000 times more computation time than the equivalent circuit model. The satisfactory match of the results was obtained for an idle operation mode.

All of the examples considered above investigate the SHM design with two stator and rotor stack combinations (SRSCs). The papers [5], [14]–[15] consider 2D methods only for the idle operation mode and do not consider operation under load.

To summarize the review mentioned above, two kinds of FEM were proposed for the evaluation of the characteristics of the SHMs. The first is 3D FEM and the second is 2D FEM where the axial and radial fluxes are evaluated using a magnetic circuit. The disadvantage of 3D FEM is the required computation resources, which makes it nearly impossible to optimize the electrical machine parameters. The disadvantage of the 2D FEM and equivalent circuits is their low accuracy: equivalent circuit models neglect details of the motor design, and 2D FEMs introduce the elements absent in reality, which distort the magnetic field picture in the motor.

This paper considers the 320 kW SHM of a 90-ton mining truck. A new approach to the 2D FEM is introduced, which helps to decrease computation time significantly compared to 3D FEMs and allows obtaining the needed parameters of machine operation. The obtained results are compared with the experimental results of a real nine-phase three-section 320 kW motor. The magnetic flux density in the transverse cross-section of the stacks is represented as two components: the excitation flux density (flux density of the magnetic monopole distributed along the rotational axis) and the flux density of the armature winding. The computational area excludes the shaft and the rotor sleeves area; therefore, not only the flux density of the armature winding satisfies the law of magnetic charges absence (the Gauss's law for magnetism), but the monopole field does as well. The peculiarities of the monopole lie out of the computational area. Therefore, compared to known 2D FEMs, in the proposed 2D model, the computational area does not contain any imaginary elements and represents the magnetic field more correctly.

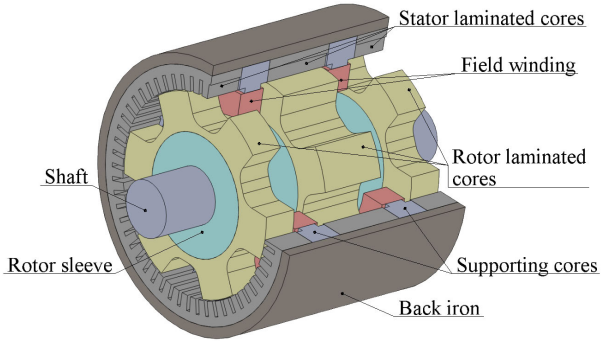

FIGURE 1. Sketch of the motor. Armature winding is not shown.

Also, the symmetry between electromagnetic processes in neighboring SRSCs is investigated in this paper, which allows predicting the torque and voltage waveforms of the whole motor by computing those for a single SRSC.

The proposed model is designed based on a magnetostatic approach with various rotor positions. For the given SHM, the SRSC symmetry has been studied to reduce the computational area and to determine the minimal range of the rotor position to be considered.

The losses in the rotor and stator cores are evaluated using postprocessing. The model allows evaluating the mechanical, active, and reactive powers, the torque waveform, etc.

II. DESIGN FEATURES OF THE SHM

3D view of the SHM with three SRSCs mounted in the motor with spans between them is shown in Fig.1. The stator stacks are mounted in the housing (back iron), and the rotor stacks are mounted on the sleeve fixed on the shaft. There are excitation windings in the spans between the SRSCs. In the slots of three stator stacks, there is a common twelve-pole armature winding (which is not shown in Fig.1 to not clutter it and can be seen in Fig. 2b). The number of teeth of each rotor stack is equal to the number of the armature winding pole pairs, $p = 6$. Since the excitation windings create opposite poles in the adjacent rotor stacks, the side rotor stacks are rotated by 180 electrical (30 mechanical) degrees with respect to the middle rotor stack. The supply frequency is defined by the rotation speed as follows: $f = p \cdot n/60$. The electrical angular frequency and mechanical angular rotational speed are $\omega = 2 \cdot \pi \cdot f$; $\Omega = 2 \cdot \pi \cdot n/60$, respectively.

The excitation magnetic flux of the middle SRSC divides into two fluxes and circuits through the side SRSCs.

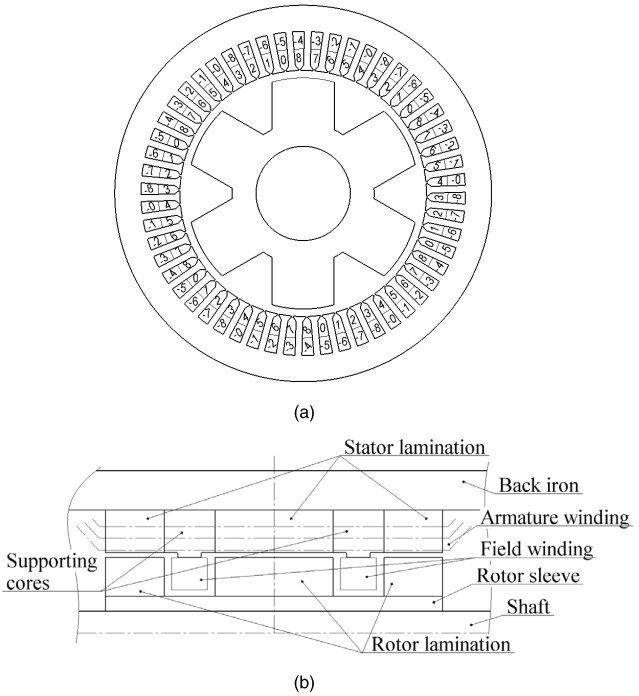

FIGURE 2. Sketch of the motor transversal (a) and axial (b) cross-sections (phases are numbered from 0 to 8).

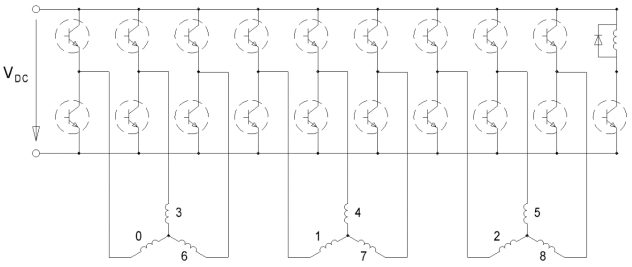

FIGURE 3. Inverter schematic.

Therefore, the middle SRSC is twice as long as the ones on the sides.

The armature winding consists of three three-phase sub-windings forming a nine-phase winding, each of which has its separate neutral point. This is done to reduce the current in each phase to simplify the design of the traction inverter. The phase shift between adjacent phases is $360°/9 = 40$ electrical degrees. The phases are marked with digits from 0 to 8 as shown in Fig. 2a. The number of the stator slots Z_s is equal to 54. The number of the stator slots per 2 poles is equal to $Z_s / p = 54/6 = 9$. The winding has two layers, and its coil pitch is four stator slots. The phase currents are supposed to be sinusoidal.

The schematic diagram of the traction inverter for the SHM is shown in Fig. 3. The inverter contains three three-phase inverters and a separate chopper for the excitation current control.

There are two sets of SRSCs, with identical orientations of the rotor stacks. The rotor stacks of one set are rotated by

TABLE 1. Main parameters of the motor.

Parameter	Value
Cross-section of the stator back iron $S_{back\ iron}$, mm^2	81400
Cross-section of the rotor sleeve S_{sleeve}, mm^2	78900
The outer radius of the stator stack, mm	331
The inner radius of the stator stack, mm	266
The total length of the SRSCs a, mm	386
The gap between SRSCs used for a field winding Δa, mm	73
The air gap, δ, mm	2.3
Cross-section of the rectangular armature wire, mm^2	3.15 x 4.5
Number of turns in the layer, n_w	5
Number of strands	2
Number of parallel-connected branches, n_{pb}	2

180 electrical degrees relative to the rotor stacks of another set. The total length of stacks of one set is approximately equal to the total length of another set. In the case of the SHM with three SRSCs, the first set consists of only the middle SRSC, and the second one consists of two lateral SRSCs.

These two SRSCs produce equal average torque and equal contribution to the active and reactive power in the case of sinusoidal armature currents. However, the instantaneous values of the torque and EMF in these SRSCs are different. Therefore, the modeling of the SHM is conducted in two stages. At first, it is assumed that the SHM has only one SRSC, whose length is equal to the sum of all SRSCs' lengths. The curves of the torque, voltages, etc., are evaluated using a set of the magnetostatic problems for various rotor angular positions. Then, the symmetrization procedure should be applied to spread the results to the real SHM.

III. BOUNDARY VALUE PROBLEMS MODELING THE MAGNETIC FIELD IN THE TRANSVERSE CROSS-SECTIONS OF THE SRSC

The assumptions made for the modeling of the magnetic field in the transverse cross-sections of the SRSC is as follows:

– The magnetic field lies on the normal plane to the axis of rotation (transverse plane, further plane XY, shaft is centered to the origin);

– The current in the armature windings flows parallel to the axis of rotation.

The equations of the static magnetic field are as follows:

$$\frac{\partial B_x}{\partial x} + \frac{\partial B_y}{\partial y} = 0, \tag{1}$$

$$\frac{\partial H_y}{\partial x} - \frac{\partial H_x}{\partial y} = J_z. \tag{2}$$

where J_z is the z-component of the current density, which is unequal to zero only in the slots filled with winding; B_x and B_y are the components of the magnetic flux density; and H_x and H_y are the magnetic field components.

The general solution of Gauss's law for magnetism (1) can then be expressed as follows:

$$B_x = \frac{\partial A_z}{\partial y} + \frac{\phi x}{2\pi(x^2+y^2)};$$
$$B_y = -\frac{\partial A_z}{\partial x} + \frac{\phi y}{2\pi(x^2+y^2)}. \quad (3)$$

The first components of these equations are conventional. The magnetic vector potential A is chosen so that only the A_z component is unequal to zero. The second parts of the equations introduce the linear density of the magnetic monopole, which simulates excitation flux. This flux flows through the shaft sleeve and stator back iron between the SRSCs and is defined as follows:

$$\Phi = \frac{a\phi}{4}, \quad (4)$$

where a is the equivalent total length of the SRSCs, and $a/4$ is the equivalent length of the side SRSC of the three-SRSC machine.

Equations (2) and (3) are complemented by the constitutive equations. Consider the calculation of the current density. The current vector $\mathbf{I}_{dq}$ in dq reference frames should be chosen as described below (23). The dq reference frame is linked to the rotor angular position, and the current vector magnitude is equal to the absolute value of the phase current. For a given rotor position, $\mathbf{I}_{dq}$ transforms into the current vector $\mathbf{I}_{xy}$ in stationary XY reference frames, and the phase currents are evaluated using the Clarke transform generalized to the case of nine phases:

$$I_n = I_x \cos\frac{2\pi n}{n_{ph}} + I_y \sin\frac{2\pi n}{n_{ph}}. \quad (5)$$

Then, the current density is evaluated as:

$$J_z = \sum_{k=0}^{n_{ph}-1} \Xi_k I_k, \quad (6)$$

where $\Xi_k(x, y)$ is the current density of the current equal to 1 A, which is flowing through a phase k, when other currents are equal to zero:

$$\Xi_k(x,y) = \begin{cases} \dfrac{n_w}{n_{pb}S_{\text{sec}}}, \ \textit{when } (x,y) \in \textit{phase } k \\ \textit{with positive direction of the current}; \\ -\dfrac{n_w}{n_{pb}S_{\text{sec}}}, \ \textit{when } (x,y) \in \textit{phase } k \\ \textit{with negative direction of the current}; \\ 0, \ \textit{otherwise}, \end{cases} \quad (7)$$

where S_{sec} is the cross-section of the SRSC.

The rotor rotates together with the rotating field, and the eddy currents are mostly absent in its iron. Since the rotor sleeve is ferromagnetic, the normal derivative of A_z is equal to zero at the inner border of the rotor stack (Neumann boundary condition).

On the contrary, magnetic flux lines are frozen in the back iron of the stator and the normal component of the magnetic field at the outer boundary of the stator lamination is represented by the field of the monopole only. Therefore, the Dirichlet boundary condition $A_z = 0$ is assumed for the outer border of the laminated stator stack.

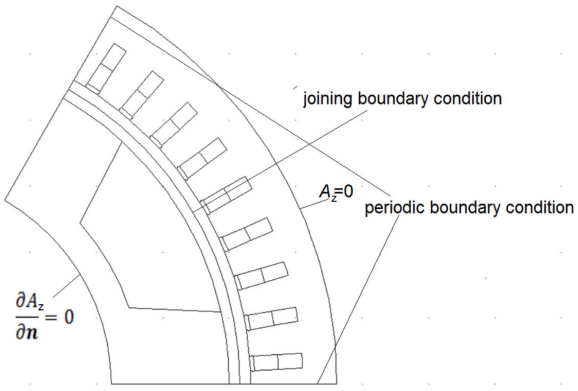

FIGURE 4. The scheme of the calculation geometry.

The same computational area (see Fig. 4) is taken for the magnetostatic tasks for various rotor positions. The computational area is a sector equal to a single electrical revolution ($360°/p$); the electrical revolution is equal to 60 mechanical degrees when the number of pole pairs p is equal to 6.

The computational area is divided into two subareas by the arc lying in the center of the air gap. The boundary condition linking magnetic vector potential at the common border of the subareas ensures the continuity of the vector potential on both sides of the arc. The correspondence of the points on both sides of the arc depends on the rotor angular position.

A periodical boundary condition ensures the equality of the magnetic vector potential at the borders, limiting the sector of the computational area by a single electrical revolution.

The SRSC is symmetric with respect to the rotor rotation by $1/n_{ph} = 1/9$ of the electrical revolution together with the cyclic transposition of the phases. During the transposition, each phase is interchanged with the next one. Therefore, it is necessary to consider only rotor positions in the range of $1/n_{ph}$ of the electrical revolution. This range is split into g equal parts, and $g+1$ boundary value problems should be solved for the following rotor positions given in electric radians:

$$\varphi_i = \frac{2\pi i}{n_{ph} g}, \quad i = 0, 1, \ldots g. \quad (8)$$

Using the considered symmetry operation, the last boundary value problem is derived from the first when the rotor is rotated by $1/n_{ph}$ of the electrical revolution, and it appears excessive. This additional boundary value problem is useful for the evaluation of the losses in the armature winding produced by eddy currents and for the stator or rotor core losses calculation. But it is necessary to remember that this excessive problem should be excluded when evaluating, for example, the average torque by averaging over g solutions with $i = 0, 1, \ldots, g-1$.

IV. CALCULATION OF EXCITATION MAGNETIC CIRCUIT OF THE SHM

Each field winding coil contains N turns and is located between the lamination stacks. The excitation current I_{exc} produces the magnetomotive force (MMF) as follows:

$$MMF = NI_{exc}. \tag{9}$$

The MMF drop at the SRSC for the rotor position i (8) is defined by the line integral through the computational area from the inner border of the rotor lamination stack to the outer border of the stator along the arbitrary path. Particularly, integration can be done along any radius:

$$F_i = \int\limits_{Any\ radius} \frac{H_{xi}x + H_{yi}y}{r} dr, \tag{10}$$

where $r = (x^2 + y^2)^{0.5}$, and the result of calculation of (10) for various radiuses can be different due to computational errors. Therefore, it is assumed that averaging the value of (10) over various radiuses gives more precise results. Its value is defined using the double integral over the entire computational area:

$$\begin{aligned} F_i &= \frac{p}{2\pi} \int\limits_0^{2\pi/p} d\alpha \int \frac{H_{xi}x + H_{yi}y}{r} dr \\ &= \frac{p}{2\pi} \iint \frac{H_{xi}x + H_{yi}y}{x^2 + y^2} dS. \end{aligned} \tag{11}$$

Since the magnetic flux lines are frozen in the back iron, the linear density of the magnetic charge is assumed to be constant in time. And the MMF drop across the SRSC matches the average value (11) over all considered rotor positions (8):

$$F = \frac{p}{2\pi g} \sum_{i=0}^{g-1} \iint \frac{H_{xi}x + H_{yi}y}{x^2 + y^2} dS, \tag{12}$$

The MMF drops for the segments of the sleeve F_{sleeve} and the back iron $F_{backiron}$ are equal to:

$$F_{sleeve} = H_{sleeve}\left(\frac{\Phi}{S_{sleeve}}\right)\Delta a\ ; \tag{13}$$

$$F_{back\ iron} = H_{back\ iron}\left(\frac{\Phi}{S_{back\ iron}}\right)\Delta a, \tag{14}$$

where H_{sleeve} and $H_{backiron}$ are the dependences of the magnetic field on the magnetic flux density in the sleeve and the back iron, respectively.

The equation of the excitation magnetic circuit is the following:

$$MMF = 2F + F_{back\ iron} + F_{sleeve}. \tag{15}$$

This equation (15), taking into account (4), (9), (12), (13), and (14), is an additional equation to the set of magnetostatic problems. This equation is consistent with the linear density of the magnetic charge ϕ, which should be found to satisfy (15).

V. CALCULATION OF AVERAGED CHARACTERISTICS OF THE SHM

Though the laminations of the rotor parts are shifted by 180 electrical degrees with respect to each other, they bring the same contribution to the (average) traction torque, the active and reactive powers, and the losses as shown in the next section. This section considers the closed system of boundary value problems and algebraic equations for the calculations of the averaged characteristics, without taking into account the rotor lamination shift. The same assumption is convenient for the calculation of the torque waveform, voltages, and flux linkages. However, it is necessary to perform the symmetrization procedure, which is described in the next section, to obtain the actual waveforms.

The torque at the shaft can be calculated by integrating the Maxwell stresses. The line integral is replaced by a double integral, which gives a higher accuracy for numerical calculations. The integral should be calculated over the cross-section of the air gap:

$$T = \frac{pa}{\delta} \iint H_\varphi B_r r dS. \tag{16}$$

The flux linked with the phase n is calculated using:

$$\Phi_n = pa \iint \Xi_n A_z dS. \tag{17}$$

In both (16) and (17), p takes into account the reduction of the computational area.

Numerical differentiating of (17) obtains the waveform of the phase voltages, and then the phase-to-phase voltages.

The period for the torque waveform is 1/9 of the electrical revolution. Since the phases are connected in three three-phase systems, the spectrum of the phase-to-phase voltage is free of the triplen harmonics.

Φ_x, Φ_y are calculated using inverse generalized Clarke transform:

$$\begin{aligned} \Phi_x &= \frac{2}{n_{ph}} \sum_{n=0}^{n_{ph}-1} \Phi_n \cos\frac{2\pi n}{n_{ph}}, \\ \Phi_y &= \frac{2}{n_{ph}} \sum_{n=0}^{n_{ph}-1} \Phi_n \sin\frac{2\pi n}{n_{ph}}. \end{aligned} \tag{18}$$

Then Φ_d and Φ_q are to be calculated. Average torque can be calculated as:

$$< T >= \frac{n_{ph}p}{2}\left(I_q < \Phi_d > - I_d < \Phi_q >\right), \tag{19}$$

where $<>$ is the averaging over g boundary value problems. Average values of torque, which are estimated using (16) and (19), are not equal due to computational errors. However, the small difference between them (of less than 0.1%) shows the correctness of the model. The average of these two values of torque estimations according to (16) and (19) is utilized for the calculation of the mechanical (active) power P excluding

losses. Moreover, the reactive power Q can be evaluated as:

$$\begin{cases} P = \Omega T; \\ Q = \dfrac{n_{ph}\omega}{2}\left(I_d < \Phi_d > + I_q < \Phi_q >\right). \end{cases} \tag{20}$$

The resistance losses in the field winding P_{exc} and in the armature winding P_{arm} can be calculated using the Joule-Lenz law. Calculation of the losses in the stator P_{stator} and rotor P_{rotor} laminations can be made similar to [16].

The eddy current losses $P_{eddyarm}$ in the armature winding are induced by the slot leakage flux crossing its wires. The wires have a rectangular cross-section and their thickness in the normal direction to the bottom of the slot (permeated by lines of slot leakage flux) is $h = 3.5$ mm. These losses averaged over the conductor volume for the flat conductor with the thickness of h are calculated using:

$$p_{eddy} = \frac{h^2\sigma}{12}\left(\frac{\partial \mathbf{B}}{\partial t}\right)^2. \tag{21}$$

Taking into account the fill factor of the slot k_z, eddy current losses in the winding $P_{eddyarm}$ can be calculated by integrating $p_{eddy}k_z$ over the volume of the stator slots.

Mechanical losses are estimated using free runout experiments and they are approximated as:

$$P_{Mech.losses} = k_1\Omega + k_3\Omega^3, \tag{22}$$

where $k_1 = 0.754$ W·s/rad, $k_3 = 0.0002348$ W·s^3/rad^3 are the friction coefficients in the ball bearings and the ventilation losses coefficient, respectively.

The losses in the stator lamination and additional losses in the armature winding are taken into account by adding a virtual current source connected in parallel to the winding. Therefore, the current vector used in calculations $\mathbf{I}_{dq}$ and represented in the rotary reference frame is expressed through the actual current vector $\mathbf{I}_{0\,dq}$ as follows:

$$\mathbf{I}_{dq} = \mathbf{I}_{0dq} - \frac{2(P_{stator} + P_{EddyArm})\mathbf{U}_{dq}}{n_{ph}\mathbf{U}_{dq}^2}, \tag{23}$$

where $\mathbf{U}_{dq}$ is the voltage vector of fundamental frequency (without considering voltage drop across phase resistance),

$$U_d = -\omega < \Phi_q >,\ U_q = \omega < \Phi_d > \text{ and } \omega = 2\pi f.$$

Since the boundary value problems are non-linear, they should be solved in several iterations. In each iteration, the value of $\mathbf{I}_{dq}$ is adjusted according to (23). Equation (23) can be considered as a recurrent equation for $\mathbf{I}_{dq}$. Thus, boundary value problems should be solved together with (23) and (15).

Losses in the rotor iron are considered as additional mechanical losses. Therefore, the mechanical and active powers are calculated as follows:

$$\begin{aligned} P_{mech} &= P - P_{rotor} - P_{Mech.losses}, \\ P_A &= P + P_{stator} + P_{EddyArm} + P_{arm}. \end{aligned} \tag{24}$$

Then, efficiency can be found with:

$$\eta = \frac{P_{mech}}{P_A + P_{exc}}. \tag{25}$$

VI. SYMMETRIZATION

This section considers the shift of the SRSC by 180 electrical degrees, which helps calculate actual waveforms of the torque and voltages based on the waveforms of torque and voltages obtained in the previous section.

Two adjacent SRSCs have the following traits: 1) the phase current is the same in both SRSCs since it is formed by the same parts of coils lying in the stator slots; 2) the drop of excitation MMF is opposite in them; 3) the rotor stacks are shifted by 180 electrical degrees.

The processes in each SRSC are symmetric with respect to simultaneous changing signs of excitation MMF and currents, wherein, the EMF induced in the stator slots also changes its sign. Upon applying the symmetry operation to the second SRSC, the following properties will be obtained: 1) the phase current is shifted by 180 degrees (due to the change of the sinusoidal current signs); 2) the MMF drop is coincidental with the first SRSC; 3) the rotor stacks are shifted by 180 electrical degrees.

In other words, the operation of symmetry reflects the processes in the second SRSC into processes in the first SRSC with a shift of 180 degrees. As mentioned above, there are two SRSC sets of equal length which produce equal average torque. Thus, the torque of the second SRSC set is equal to the torque of the first SRSC set with a shift of 180 degrees, while the voltages have opposite signs. Therefore, after the calculation of the torque and voltage waveforms, supposing that the motor contains only one SRSC of the total length of three SRSCs, symmetrization must be performed:

$$\begin{aligned} T_{sym} &= \left(T(t) + T\left(t + \frac{\tau}{2}\right)\right)/2\,; \\ U_{sym} &= \left(U(t) - U\left(t + \frac{\tau}{2}\right)\right)/2\,. \end{aligned} \tag{26}$$

where U and T are the phase voltage and the torque before the symmetrization and τ is the electrical period.

No limitations to the number of parts g of the interval of the considered rotor positions were specified till now. Now, this number g should be even. Then, the shift by half of the electrical revolution can be performed by adding $g/2$ to the index of the data arrays (the next element for the last element is assumed to be the first element). However, phase voltage cannot be measured for the motors in which neutral points are not available. The waveform of the phase-to-phase voltage is evaluated using the following equation:

$$U_{line} = U_{sym}(t) - U_{sym}\left(t + \frac{2\tau}{3}\right). \tag{27}$$

Therefore, it is better to take g in multiples of 2 and 3, or multiples of 6. Then, the shift by 2/3 of the electrical revolution is done by adding $2g/3$ to the index of the data arrays. The torque period was reduced from 1/9 to 1/18 as a result of the symmetrization procedure. Moreover, not only triplen voltage harmonics are unobservable, but even voltage harmonics are unobservable as well. Thus, the existing harmonics after the symmetrization are $6l+1$, where l is the integer number.

VII. COMPUTATION AND EXPERIMENTAL RESULTS

Two experimental prototypes of the considered motor design were tested using the dual supply back-to-back method (2-1-1D method according to IEC 60034-2-1-2014). Fig. 5 shows the SHM prototype used in the experiments, and its rotor is shown in Fig. 6. One of the SHMs operates in the braking (generator) mode, creating the load for another SHM operating in the motor mode. The inverters of both machines which schematic is shown in Fig.3 were connected to the common DC-link. As a result, the power consumed from DC-link is equal only to the total losses in the SHMs and the inverters. The machines were tested with external air cooling. Fig. 7 shows the testbench with the two traction SHMs and two inverters of the powertrain of a mining truck.

The electrical power of both SHMs is measured using the power analyzer. The difference between the active motor power and the active generator power is the sum of the power losses in two identical machines operating at the same rotational speed and producing the same torque. Assuming that the losses in both SHMs are the same, the total losses in each can be calculated as well as the mechanical shaft power.

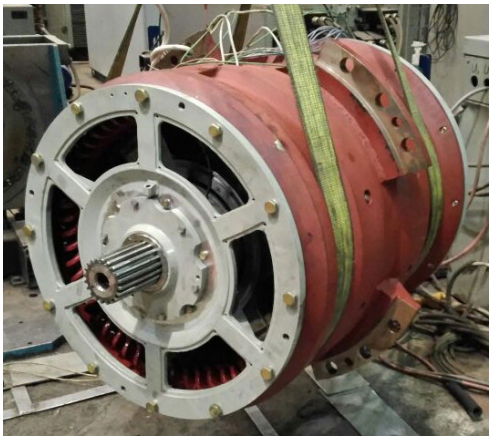

FIGURE 5. SHM experimental prototype.

FIGURE 6. Rotor of the experimental prototype.

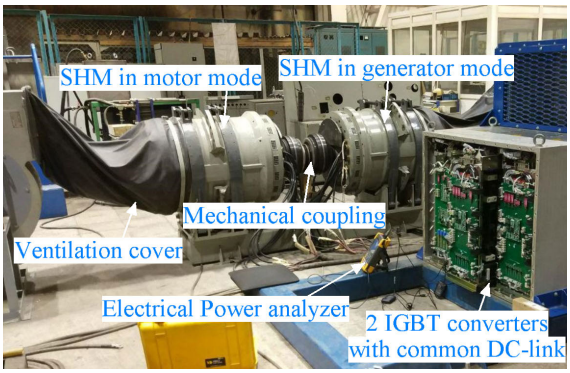

FIGURE 7. Testing the motor prototypes.

TABLE 2. Operation mode parameters of the SHM.

Mode Number	1	2	3	4	5
Speed, rpm	3102	2440	1443	1420	1400
Armature current, A, ampl.	174	195	253	286	271
Excitation current, A	5.6	6.4	9.2	7.6	9
Control angle, el. Degrees	24	15	0	0	0
Active power, kW	329.1	340.2	332.0	325.7	339.0
Torque ripple before symmetrization, %	69.4	69.8	66.9	67.7	66.5
Torque ripple after symmetrization, %	22.2	19.3	15.1	14.7	14.7
Mechanical losses, kW	8.29	4.11	0.92	0.88	0.85
Resistance armature winding losses, kW	1.46	1.84	3.09	3.95	3.54
Eddy-current armature winding losses, kW	2.84	2.56	2.12	2.02	2.13
Excitation winding losses, kW	0.39	0.51	1.06	0.72	1.01
Mechanical losses, kW	8.29	4.11	0.92	0.88	0.85
Stator core losses, kW	10.41	9.57	7.08	6.62	6.82
Rotor core losses, kW	1.95	1.75	1.10	0.90	1.01
Computed motor efficiency, %	92.3	94.0	95.4	95.4	95.5
Power factor (under the first harmonic)	0.985	0.962	0.923	0.852	0.907
Computed efficiency of the inverter, %	97.4	97.2	96.9	96.8	96.8
Computed efficiency of the drive including inverter and motor, %	89.9	91.4	92.4	92.3	92.4
Measured efficiency of the drive including inverter and motor, %	89.7	92.3	91.6	91.6	90.8
Motor mechanical power, kW (computed)	304.1	320.4	317.7	311.3	324.6
Motor mechanical power, kW (experimental)	324.7	332.0	324.7	322.5	319.4

Table 2 demonstrates some operation modes of the SHM observed in the experiment. The excitation current, the armature winding current, and the current angle in these modes were used to carry out the computations. The computation results are also provided in Table 2 for the comparison.

The speeds in the last three modes are approximately equal. The efficiency and the torque ripple are approximately equal

FIGURE 8. The mining truck with two SHMs as rear-wheel motors.

in these three modes, which shows that it is possible to adjust operation conditions to avoid the voltage or current limit. Namely, depending on excitation current, the armature winding current takes the values from 253 A ampl. to 286 A ampl.

The symmetrization procedure is needed to compute the waveforms of the torque and the voltages. Table 2 shows that the torque ripple of the SHM (after the symmetrization) is more than thrice as less than the torque ripple of the single SRSC (before the symmetrization).

Table 2 also represents the experimental and calculated efficiency of the SHM drive (efficiency of the inverter and the motor). Besides, a comparison of the computed and experimental motor mechanical power is provided in Table 2. The experimental SHM mechanical power differs from the computed one by less than 7%. The difference between the computed and experimental efficiencies of the drive (including the convertor and the SHM) is less than 1.6%. The developed mathematical model can be used in designing SHMs.

The power factor under the first (fundamental) harmonic is also provided in Table 2. It can be rather high at proper adjusting the control angle and the excitation current.

The eddy-current losses in the armature winding are comparable with its resistance losses and grow with the growth of the motor speed, which should be taken into account during thermal calculations of the winding behavior.

Two SHMs were used as rear-wheel motors of mining truck BELAZ 75570 (Fig. 8) to replace induction motors (IM) used earlier. The SHMs have identical dimensions and specific characteristics as the IMs. The identical forced-air cooling systems with the same power consumption are used for the SHMs and the IMs. The main advantage of traction SHMs over traction IMs is their high reliability. A more detailed comparison of SHM with other traction motors for the mining truck will be done in further papers.

VIII. CONCLUSION

In this paper, a novel 2D FEM of the SHM is proposed. The FEM uses the general solution of the Gauss's law for magnetism containing the excitation flux represented by the magnetic monopole field. Since the magnetic monopole is located outside the computational area, the computational area does not contain any imaginary elements distorting the magnetic field picture. The symmetry between electromagnetic processes in neighboring stator and rotor stack combinations (SRSCs) is investigated in the paper, which allows predicting the torque and voltage waveforms of the whole motor by computing those for a single SRSC. The SRSC symmetry also is studied to reduce the computational area and to determine the necessary range of rotor position to be considered. The model is based on a set of magnetostatic boundary value problems for various rotor positions, solved with the finite element method. The set of boundary problems is completed with the excitation equivalent circuit. The losses in the armature and field windings, as well as in the stator and rotor magnetic cores are computed in postprocessing.

A comparison of the theoretical and experimental data for nine-phase three-section 320 kW SHM is carried out. These SHMs were used as rear-wheel motors in a mining truck with a carrying capacity of 90 tons. High reliability of the proposed SHM was validated during its two-year operation as part of the powertrain of the electric mining truck. As a result, the proposed SHMs can be recommended for replacing traction induction motors in hybrid electric mining vehicles of this kind.

REFERENCES

[1] C. Ye, J. Yang, F. Xiong, and Z. Q. Zhu, "Relationship between homopolar inductor machine and wound-field synchronous machine," *IEEE Trans. Ind. Electron.*, vol. 67, no. 2, pp. 919–930, Feb. 2020, doi: 10.1109/TIE.2019.2898577.

[2] G. R. Bindu, J. Basheer, and A. Venugopal, "Analysis and control of rotor eccentricity in a train-lighting alternator," in *Proc. IEEE Int. Conf. Power, Control, Signals Instrum. Eng. (ICPCSI)*, Chennai, India, Sep. 2017, pp. 2021–2025, doi: 10.1109/ICPCSI.2017.8392070.

[3] C. Bianchini, F. Immovilli, A. Bellini, E. Lorenzani, C. Concari, and M. Scolari, "Homopolar generators: An overview," in *Proc. IEEE Energy Convers. Congr. Expo.*, Phoenix, AZ, USA, Sep. 2011, pp. 1523–1527, doi: 10.1109/ECCE.2011.6063962.

[4] K. Yu, J. Yao, X. Xie, and P. Tang, "A novel critical analysis method of homopolar inductor alternator for preliminary design in capacitor charge power supply," *IEEE Trans. Plasma Sci.*, vol. 47, no. 5, pp. 2354–2361, May 2019, doi: 10.1109/TPS.2019.2892610.

[5] E. Severson, R. Nilssen, T. Undeland, and N. Mohan, "Magnetic equivalent circuit modeling of the AC homopolar machine for flywheel energy storage," *IEEE Trans. Energy Convers.*, vol. 30, no. 4, pp. 1670–1678, Dec. 2015, doi: 10.1109/TEC.2015.2441040.

[6] M. Lashkevich, A. Anuchin, D. Aliamkin, and F. Briz, "Control strategy for synchronous homopolar motor in traction applications," in *Proc. IECON 43rd Annu. Conf. IEEE Ind. Electron. Soc.*, Beijing, China, Oct. 2017, pp. 6607–6611, doi: 10.1109/IECON.2017.8217153.

[7] N. Sugitani, A. Chiba, and T. Fukao, "Characteristics of a doubly salient-pole homopolar machine in a constant-power speed range," in *Proc. Conf. Rec. IEEE Ind. Appl. Conf. 33rd IAS Annu. Meeting*, St. Louis, MO, USA, vol. 1, Oct. 1998, pp. 663–670, doi: 10.1109/IAS.1998.732399.

[8] S.-H. Lee, J.-P. Hong, Y.-K. Kwon, Y.-S. Jo, and S.-K. Baik, "Study on homopolar superconductivity synchronous motors for ship propulsion applications," *IEEE Trans. Appl. Supercond.*, vol. 18, no. 2, pp. 717–720, Jun. 2008, doi: 10.1109/TASC.2008.921334.

[9] E. Severson, R. Nilssen, T. Undeland, and N. Mohan, "Dual-purpose no-voltage winding design for the bearingless AC homopolar and consequent pole motors," *IEEE Trans. Ind. Appl.*, vol. 51, no. 4, pp. 2884–2895, Jul./Aug. 2015, doi: 10.1109/TIA.2015.2388852.

[10] J.-S. Jeong, D.-K. An, J.-P. Hong, H.-J. Kim, and Y.-S. Jo, "Design of a 10-MW-Class HTS homopolar generator for wind turbines," *IEEE Trans. Appl. Supercond.*, vol. 27, no. 4, Jun. 2017, Art. no. 5202804, doi: 10.1109/TASC.2017.2669140.
[11] H. M. Cheshmehbeigi and E. Afjei, "Design optimization of a homopolar salient-pole brushless DC machine: Analysis, simulation, and experimental tests," *IEEE Trans. Energy Convers.*, vol. 28, no. 2, pp. 289–297, Jun. 2013, doi: 10.1109/TEC.2013.2249584.
[12] E. Severson, N. Mohan, R. Nilssen, and T. Undeland, "Outer-rotor AC homopolar motors for flywheel energy storage," in *Proc. 7th IET Int. Conf. Power Electron., Mach. Drives (PEMD)*, Manchester, U.K., 2014, pp. 1–6, doi: 10.1049/cp.2014.0345.
[13] J. Yang, C. Ye, X. Liang, W. Xu, F. Xiong, Y. Xiang, W. Li, "Investigation of a two-dimensional analytical model of the homopolar inductor alternator," *IEEE Trans. Appl. Supercond.*, vol. 28, no. 3, Apr. 2018, Art. no. 5205205, doi: 10.1109/TASC.2018.2802480.
[14] Q. Wang, C. Liu, J. Zou, X. Fu, and J. Zhang, "Numerical analysis and design optimization of a homopolar inductor machine used for flywheel energy storage," *IEEE Trans. Plasma Sci.*, vol. 41, no. 5, pp. 1290–1294, May 2013, doi: 10.1109/TPS.2013.2243847.
[15] C. Belalahy, I. Rasoanarivo, and F. M. Sargos, "Using 3D reluctance network for design a three phase synchronous homopolar machine," in *Proc. 34th Annu. Conf. IEEE Ind. Electron.*, Orlando, FL, USA, Nov. 2008, pp. 2067–2072, doi: 10.1109/IECON.2008.4758275.
[16] V. Dmitrievskii, V. Prakht, V. Kazakbaev, S. Oshurbekov, and I. Sokolov, "Developing ultra premium efficiency (IE5 class) magnet-free synchronous reluctance motor," in *Proc. 6th Int. Electric Drives Prod. Conf. (EDPC)*, Nuremberg, Germany, Nov. 2016, pp. 2–7, doi: 10.1109/EDPC.2016.7851306.

VLADIMIR DMITRIEVSKII received the master's degree in theoretical physics and the Ph.D. degree from Ural Federal University, Yekaterinburg, Russia, in 1996 and 2007, respectively, and the Ph.D. degree in mathematical modeling and optimal designing the linear electric motors, in 2006. He is currently an Associate Professor with the Department of Electrical Engineering, Ural Federal University. His research interests include optimal designing energy-efficient motors and developing sensorless control algorithms for electric drives.

VLADIMIR PRAKHT (Member, IEEE) received the bachelor's degree in engineering and the Ph.D. degree from the Department of Electrical Engineering, Ural Federal University, Yekaterinburg, Russia, in 2004 and 2007, respectively, and the Ph.D. degree in optimal control and mathematical modeling induction heating systems, in 2006. He is currently an Associate Professor with the Department of Electrical Engineering, Ural Federal University. His research interests include mathematical modeling and optimal design of energy efficient electric motors and generators.

ALECKSEY ANUCHIN (Senior Member, IEEE) received the B.Sc., M.Sc., Ph.D., and Dr.Eng.Sc. degrees from the Moscow Power Engineering Institute, Moscow, Russia, in 1999, 2001, 2004, and 2018, respectively. He delivers lectures on "control systems of electric drives," "real-time software design," "electric drives," and "science research writing" at the Moscow Power Engineering Institute. He has been in a head position with the Electric Drives Department for the last eight years. He has more than 20 years of experience covering control systems of electric drives, hybrid powertrains, and real-time communications. He is the author of three textbooks on the design of real-time software for the microcontroller of the C28 family and Cortex-M4F, and control system of electric drives, in Russian. He has authored or coauthored more than 100 conference and journal papers.

VADIM KAZAKBAEV received the bachelor's degree in engineering and the Ph.D. degree from the Department of Electrical Machines, Ural Federal University, Yekaterinburg, Russia, in 2010 and 2017, respectively, and the Ph.D. degree in development of high-performance synchronous reluctance motor, in 2016. He is currently a Junior Researcher and an Associate Professor with the Department of Electrical Engineering, Ural Federal University. His research interests include electrical engineering, design of electrical machines, and control of electrical drives.